Hydrogen Bonding and Intermolecular Vibrations of 7-Hydroxyquinoline·NH_3 in the S_0 and S_1 States

Stéphane Coussan, Andreas Bach, and Samuel Leutwyler*

Departement für Chemie und Biochemie, Universität Bern, Freiestrasse 3, CH-3000 Bern 9, Switzerland

Received: February 10, 2000; In Final Form: August 1, 2000

7-Hydroxyquinoline·$(NH_3)_n$ microsolvent clusters have been shown to exhibit excited-state proton transfer (ESPT) in the S_1 state for $n \geq 4$ [Bach, A.; Leutwyler, S. *J. Chem. Phys*. **2000**, *112*, 560.]. We present a combined spectroscopic and ab initio theoretical investigation of the first member of this cluster series, the hydrogen-bonded 7-hydroxyquinoline·NH_3 (7-HQ·NH_3) complex. Mass- and rotamer-resolved $S_1 \leftrightarrow S_0$ vibronic spectra of supersonic jet-cooled 7-HQ·NH_3 were obtained by two-color resonant two-photon ionization and dispersed fluorescence spectroscopy. Both the trans and cis rotamers are present in the jet, at a trans/cis ratio of 1:40. The H-bond vibrations σ (stretch), β_1 and β_2 (in-plane wagging), and τ (NH_3 hindered internal rotation) were observed in the S_0 and S_1 states. Ab initio calculations using Hartree−Fock (SCF) and hybrid density functional (B3LYP) methods for the S_0 state and the configuration interaction singles (CIS) method for the S_1 state yield C_s symmetric equilibrium structures with nearly linear O−H···NH_3 H-bonds. Agreement between the B3LYP/6-311++G(2d,2p) calculated vibrational frequencies and experimental S_0-state frequencies is very good for both inter- and intramolecular modes. The ground-state effective internal rotation barrier of the NH_3 group about its C_3 axis was determined as $V_3(S_0) = 73$ cm^{-1}. $S_1 \leftarrow S_0$ excitation leads to contraction of the R(O···N) distance by −0.062 Å, accompanied by an increase of the H-bond dissociation energy by 2.62 kcal/mol and an increase of the NH_3 internal rotation barrier to $V_3(S_1) = 88$ cm^{-1}. The H-bond contraction is in agreement with the SCF and CIS ab initio calculations which predict ΔR(O···N) = −0.053 Å. These calculations predict large intramolecular geometric changes which are not directly along the proton-transfer coordinate.

1. Introduction

Among the conceptually simplest chemical reactions is the transfer of a proton from an acid A−H to a base B. The investigation of intermolecular proton-transfer reactions in jet-cooled collision-free microsolvent clusters A−H·B_n has allowed the study of this paradigmatic reaction in a "minimum solvent environment" and at low temperatures.[1−8] By electronic excitation to low-lying electronic states, the acidity of hydroxyaromatic molecules such as 1- or 2-naphthol can be strongly increased, giving pK_a decreases of 6−9 units.[9−11] Photoinitiated acid−base reactions of the excited-state acids phenol, 1-naphthol, and 2-naphthol attached to microsolvent clusters of the bases NH_3, methylamine, ethylamine, and piperidine have been studied.[1−8,12−24]

7-Hydroxyquinoline (7-HQ) is a bifunctional aromatic molecule: in its enol form (see Figure 1), it acts as a proton donor at the O−H group and as a proton acceptor at the N atom.[25,26] As for 1- and 2-naphthol, electronic excitation to the S_1 state strongly modifies the acid−base properties of this molecule, rendering the hydroxyl group more acidic and the N atom more basic.[25−30] Excited-state pK_a values of 3.5 and −2.7 have been determined by the Förster cycle from the absorption and emission spectra, respectively.[25] In protic solvents, adiabatic S_1 excited-state proton transfer (ESPT) can occur from the O−H group of 7-HQ to the solvent and from the solvent to the quinoline N, leading to the keto tautomeric form (see Figure 1). Depending on pH and solvent, *ground*-state protonation, deprotonation, and tautomerization reactions of 7-HQ can also occur. The different ground- and excited-state forms of 7-HQ have been extensively investigated by both absorption and fluorescence spectroscopy,[25,26] by picosecond kinetic measurements,[27−30] and also in low-temperature matrices.[31−34] Most microscopic models proposed for solvent-assisted ESPT involve a *proton relay* operating between the O−H group and the N atom, mediated by several solvent molecules and coupled to the formation of either the zwitterion or keto tautomers of 7-HQ.[27−34]

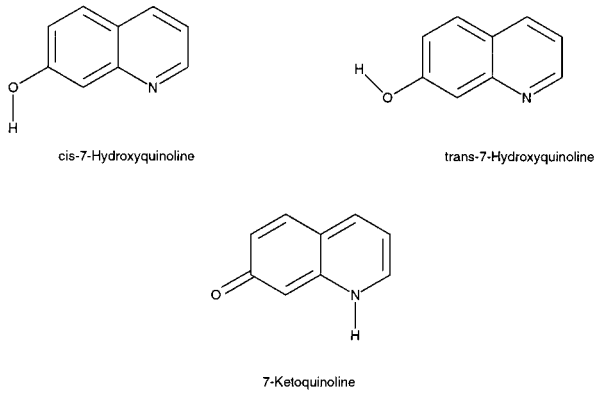

Figure 1. The *cis*- and *trans*-7-hydroxyquinoline rotamers and the 7-ketoquinoline tautomer.

Lahmani et al. investigated 7-HQ·$(H_2O)_n$/$(D_2O)_n$ clusters using laser fluorescence excitation and emission spectroscopy in supersonic jets.[35] They reported spectra of the *trans*- and *cis*-7-HQ and 7-HQ·H_2O rotamers, which differ in the orientation of the O−H bond with respect to the hydroxyquinoline frame

10.1021/jp000530h CCC: $19.00
Published on Web 10/14/2000

TABLE 1: Ab Initio Calculated Total Energies (in au), Interaction Energies ΔE_i, BSSE Contributions, and Dissociation Energies D_0 (in kcal/mol) of the *cis*-7-Hydroxyquinoline·NH_3 and 7-Ketoquinoline·NH_3 Complexes, Using the SCF/6-31G(d,p) and B3LYP/6-311++G(2d,2p) Methods

	cis-7-HQ·NH_3		7-KQ(O···H_3N)	7-KQ(N−H···NH_3)
	SCF 6-31G(d,p)	B3LYP 6-311++G(2d,2p)	SCF 6-31G(d,p)	SCF 6-31G(d,p)
$-E_{total}$ (au)	530.434 387	533.898 063	530.401 879	530.407 089
ΔE_{SCF}	−9.23	−8.92	−5.77	−9.03
δE_{BSSE}(7-HQ)[a]	0.19	0.13	0.91	0.14
δE_{BSSE}(NH_3)[a]	0.89	0.24	0.63	0.83
ΔE_{BSSE}(total)	1.08	0.37	1.54	0.97
ΔE_{CP}[b]	−8.15	−8.55	−4.23	−8.06
D_0[c]	−6.29	−6.78	−2.63	−6.42

[a] BSSE contribution of the subunits. [b] $\Delta E_{CP} = \Delta E_{SCF} + \Delta E_{BSSE}$(total). [c] $D_0 = \Delta E_{CP} + \Delta$ZPE.

(see Figure 1), and of the *cis*-7-HQ·$(H_2O)_3$ cluster. They did *not* find evidence for either solvent-assisted ESPT or tautomerization reactions in the 7-HQ·$(H_2O)_n$ clusters. Recently, mass- and isomer-selected $S_1 \leftarrow S_0$ resonant two-photon ionization and $S_1 \rightarrow S_0$ fluorescence spectra were obtained in our laboratory for the supersonically cooled 7-hydroxyquinoline·$(NH_3)_n$ clusters with $n = 2-16$.[36,37] The absorption and emission spectra of the clusters with $n = 1-3$ exhibit discrete narrow-band vibronic structure, characteristic of hydrogen-bond vibrations of neutral clusters. For $n \geq 4$, the $S_1 \leftarrow S_0$ resonant two-photon ionization (R2PI) spectra are partially or entirely broadened and strongly shifted to the red, and the $n = 4-7$ clusters show spectroscopic signatures of S_1-state enol $\rightarrow$ keto tautomerization.[36,37] For the $n \geq 7$ clusters, the absorption and fluorescence spectra correspond to those of the ground-state 7-HQ anion and the ground-state keto tautomer, which implies that *ground-state* proton-transfer reactions take place in the cluster.[37] To analyze and understand the spectra of the large clusters and the excited- and ground-state proton-transfer processes, one first needs to understand the narrow-band vibronic spectra of the smaller clusters.

Here, we present a combined theoretical and laser spectroscopic study of the 7-hydroxyquinoline·NH_3 complex. Among the issues we address are the following:

(1) The existence and relative concentrations of the enol and keto tautomers and the trans/cis rotamers[35,36,38,39] of 7-HQ·NH_3 in the supersonic jet.

(2) The hydrogen-bonding topologies of these complexes. Referring to Figure 1, we note that the *cis*-7-HQ rotamer can form three different H-bonded complexes: with 7-HQ as a donor and NH_3 as an acceptor (7-HQ-O−H···NH_3), with NH_3 as a proton donor to the quinoline N atom (NH_3···N), or with NH_3 as a proton donor to the hydroxy O atom (NH_3···O−H). The *trans*-7-HQ rotamer can form three analogous complexes, and 7-ketoquinoline (7-KQ) can act either as a proton donor at the N−H group or as an acceptor at the C═O group, potentially yielding eight different H-bonded complexes.

(3) The S_0- and S_1-state hydrogen-bond vibrations of these species and their frequencies. How strongly do they couple to the $S_1 \leftrightarrow S_0$ vibronic transitions, and how does the H-bond potential change as a function of electronic state? Which properties of the H-bonded 7-HQ·NH_3 complexes might be important with respect to the acid−base reaction between 7-HQ and larger ammonia clusters?

7-Hydroxyquinoline·NH_3 is expected to be related to the *trans*- and *cis*-2-naphthol·NH_3 and *trans*-1-naphthol·NH_3 complexes, for which Pratt and co-workers[40,41] have carefully determined the ground- and excited-state rotational constants, NH_3 internal rotation barriers, and H-bond geometries by laser fluorescence excitation spectroscopy at rotational resolution. We compare the properties of 7-hydroxyquinoline·NH_3 to those of these naphthol·NH_3 complexes.

2. Theoretical Methods and Results

2.1. Computational Procedure. Full geometry optimizations were performed for the S_0 state at the SCF level using the 6-31G(d,p) and 6-311++G(2d,2p) basis sets. The results discussed below and previous experience[42,43] show that the 6-31G(d,p) basis set is an effective optimum for the treatment of H-bonding at the SCF level. It is desirable to employ a method such as MP2, which includes the electron correlation energy. However, the MP2 method combined with even medium-sized basis sets leads to large basis set superposition errors (BSSEs); on the other hand, the calculation of MP2 frequencies with large basis sets is prohibitive for a system of the size of 7-hydroxyquinoline·NH_3. We employed density functional (DFT) methods; the B3LYP hybrid density functional in combination with the 6-311++G(2d,2p) basis set has been shown to give accurate results for H-bonded systems, exhibits small BSSE,[44] and allows harmonic frequencies to be efficiently calculated. For the S_1 excited state, we employed the configuration interaction singles (CIS) method[45] with the 6-31G(d,p) basis. The most stringent optimization criteria ($<10^{-6}$ au for the gradient norm) were employed throughout. The full counterpoise (CP) procedure was used to correct all interaction energies, ΔE, for BSSE.[46,47]

Normal mode calculations were carried out at the minimum-energy geometries. The *intra*molecular SCF vibrational frequencies were scaled to account for the overestimate of vibrational frequencies at the SCF level, using the factor 0.9028 previously determined for phenol.[42] The *inter*molecular frequencies and *all* DFT frequencies remained unscaled. The dissociation energy D_0 at each level of calculation was calculated by subtracting the scaled or unscaled harmonic vibrational zero-point energies from the CP-corrected ΔE values. All ab initio calculations were performed using the Gaussian 94 program.[45]

2.2. Calculated Interaction and Dissociation Energies. The SCF/6-31G(d,p) and B3LYP/6-311++G(2d,2p) total energies, interaction energies ΔE, dissociation energies D_0, and BSSE corrections are given in Table 1 for the *cis*-7-HQ·NH_3 rotamer and for both isomers of 7-ketoquinoline·NH_3, with 7-KQ acting as a proton donor or a proton acceptor. The CP-corrected interaction energies for the *cis*-7-HQ·NH_3 were calculated to be $\Delta E_{CP} = -8.15$, -6.50, and -8.55 kcal/mol at the SCF/6-31G(d,p), SCF/6-311++G(2d,2p), and B3LYP/6-311++G(2d,2p) levels, respectively.

For *cis*-7-HQ·NH_3 at the SCF level, the BSSE decreases with increasing basis set size, from 1.08 kcal/mol (11.7% of ΔE_{SCF}) with the 6-31G(d,p) basis set to 0.30 kcal/mol (4.4% of ΔE_{SCF})

with the 6-311++G(2d,2p) basis set. However, as the BSSE decreases at the SCF level, the interaction energy ΔE_{CP} also decreases. When correlation energy is included with the B3LYP density functional, both the CP-uncorrected and CP-corrected interaction energies increase by ~2 kcal/mol relative to the SCF/6-311++G(2d,2p) calculation. The total BSSE remains small (0.37 kcal/mol) at the B3LYP level, amounting to a 4% correction on ΔE_{SCF}. On the basis of the inclusion of electron correlation combined with small BSSE, we consider the B3LYP calculation to give the most accurate results of the three calculations. The dissociation energies D_0 are 23% and 20% smaller than ΔE_{CP} at the SCF/6-31G(d,p) and B3LYP/6-311++G(2d,2p) levels, respectively. These substantial corrections for vibrational zero-point energy are typical for hydrogen bonds.

7-Ketoquinoline acting as a N−H proton donor forms a strong H-bond to NH_3. The CP-corrected SCF/6-31G(d,p) interaction energy is $\Delta E_{CP} = -8.06$ kcal/mol, only 0.1 kcal/mol lower than that of *cis*-7-HQ·NH_3, and the D_0 of 7-KQ···NH_3 is even larger than that of *cis*-7-HQ···NH_3. However, 7-ketoquinoline is itself less stable than the 7-hydroxyquinoline tautomer; the *total* energy of 7-KQ·NH_3 lies 17.1 kcal/mol above that of *cis*-7-HQ·NH_3 (see Table 1). The 7-KQ·NH_3 isomer with NH_3 acting as a proton donor to C═O is less strongly bound, and its total energy is 20.4 kcal/mol above that of *cis*-7-HQ·NH_3. Thus, the SCF calculations predict that both isomers of the 7-KQ tautomer are energetically disfavored relative to *cis*-7-HQ·NH_3.

A low-lying transition structure (TS) along the NH_3 internal rotation coordinate τ was found, corresponding to a rotation of 60° about the C_3 axis of the NH_3 figure axis (see also the τ vibration below). Optimization to this saddle point was performed using analytical derivatives at the SCF/6-31G(d,p) level. Experimentally, we find that the population of the *trans*-7-hydroxyquinoline·NH_3 complex in the supersonic jet is very low (see Section 3). The ab initio results obtained for this rotamer will not be presented here; for details, contact the authors.

The H-bond dissociation energies D_0 of the closely related *trans*-1-naphthol·NH_3 and *trans*-d_3-1-naphthol·ND_3 complexes have been determined experimentally as $D_0 = -7.66 \pm 0.01$ and -8.01 ± 0.04 kcal/mol, respectively.[48] These experimental values can be compared to the SCF/6-31G(d,p) calculated values of $D_0 = -7.06$ kcal/mol for 1-naphthol·NH_3 and −7.47 kcal/mol for 1-naphthol·ND_3,[48] which are 0.54−0.60 kcal/mol smaller. If we assume that this difference between ab initio calculation and experiment for the 1-naphthol·NH_3 complexes is approximately transferable to *cis*-7-HQ·NH_3, we obtain from the SCF/6-31G(d,p) value of $D_0 = -6.07$ kcal/mol a "corrected" D_0 of −6.6 to −6.7 kcal/mol. The B3LYP value of $D_0 = -6.83$ kcal/mol for *cis*-7-HQ·NH_3 is close to this corrected value. On the other hand, the SCF/6-311++G(2d,2p) value is only $D_0 = -4.00$ kcal/mol, which seems unrealistically low.

2.3. Calculated Ground-State and Excited-State Equilibrium and Transition Structures. The minimum-energy equilibrium structures of all isomers and rotamers of 7-HQ·NH_3 and 7-KQ·NH_3 were found to be C_s symmetric in all calculations (SCF, B3LYP, and CIS) for both the S_0 and S_1 states, with the ammonia N and one of its H atoms lying in the molecular plane of 7-HQ. The O−H···N H-bond is only very slightly nonlinear; the angle $\varphi(H_O-O\cdots N)$ (for atom labels, see Figure 2) is predicted to be between 3.9 and 5.1°, depending on the level of theory. Important structural parameters characterizing the hydrogen-bond arrangement are compiled in Table 2. The calculated S_0-state H-bond length R(O···N) is 2.93 Å at the SCF/6-31G(d,p) level and 2.84 Å with the B3LYP/6-311++G(2d,2p) method. The shorter H-bond predicted by the DFT method agrees with the larger calculated H-bond interaction energy ΔE_{CP}; cf. Tables 1 and 2.

TABLE 2: Calculated Structural Parameters, Rotational Constants, and Dipole Moments for the *cis*-7-Hydroxyquinoline·NH_3 Complex in the S_0-State Equilibrium and Internal Rotation Transition Structure (TS), and the S_1-State Equilibrium Structure[a]

	6-31G(d,p)			6-311++G(2d,2p)
	SCF		CIS	B3LYP
parameters[b]	S_0	TS	S_1	S_0
Distances (Å)				
$R(O\cdots N_2)$	2.932	2.935	2.879 (−0.053)	2.835
$R(H_O\cdots N_2)$	1.978	1.984	1.923 (−0.055)	1.855
$r(C_7-O)$	1.335	1.336	1.316 (−0.019)	1.351
$r(O-H_O)$	0.957	0.956	0.961 (+0.003)	0.986
$r(N_2-H_{2,1})$	1.001	1.002	1.002 (+0.001)	1.014
$r(N_2-H_{2,2})$	1.007	1.001	1.006 (−0.001)	1.014
$r(N_1-C_2)$	1.295	1.295	1.329 (+0.034)	1.315
$r(C_2-C_3)$	1.413	1.413	1.392 (−0.021)	1.411
$r(C_3-C_4)$	1.360	1.360	1.402 (+0.042)	1.372
$r(C_4-C_{10})$	1.411	1.411	1.401 (−0.010)	1.409
$r(C_{10}-C_5)$	1.422	1.422	1.414 (−0.008)	1.418
$r(C_5-C_6)$	1.353	1.353	1.393 (+0.040)	1.366
$r(C_6-C_7)$	1.424	1.424	1.386 (−0.038)	1.420
$r(C_7-C_8)$	1.363	1.363	1.436 (+0.073)	1.379
$r(C_8-C_9)$	1.416	1.416	1.383 (−0.033)	1.412
$r(C_9-N_1)$	1.356	1.356	1.346 (−0.010)	1.364
$r(C_9-C_{10})$	1.408	1.408	1.456 (+0.048)	1.429
Angles (deg)				
$\varphi(H_O-O\cdots N_2)$	3.9	5.1	4.7	5.2
$\theta(C_7-O-H_O)$	112.2	112.3	113.5	111.7
$\theta(H_{2,1}-N_2\cdots O)$	105.3	107.1	104.6	105.9
$\theta(H_{2,2}-N_2\cdots O)$	114.1	119.1	114.6	114.4
$\theta(H_{2,3}-N_2\cdots O)$	114.1	107.1	114.6	114.4
$\delta(C_7-O\cdots N)$	116.1	117.4	118.2	117.0
Dihedral Angles (deg)				
$\tau(H_8-O-C_8-C_7)$	0.0	0.0	0.0	0.0
$\tau(N\cdots H_O-O-C_7)$	0.0	179.98	179.98	0.0
$\omega(H_{2,1}-N-2\cdots O-C_7)$	0.0	122.4	179.96	0.0
$\omega(H_{2,2}-N_2\cdots O-C_7)$	62.1	0.0	62.5	62.2
$\omega(H_{2,3}-N_2\cdots O-C_7)$	−62.1	−122.3	−62.6	−62.2
Rotational Constants (MHz)				
A	1762.8	1775.0	1708.1 (−54.7)	1784.1
B	563.4	557.6	575.5 (+12.1)	559.4
C	427.9	425.3	431.4 (+ 3.5)	426.8
Dipole Moment (D)				
$\|\mu\|$	1.88	1.87	3.32 (+1.44)	

[a] The SCF, B3LYP, and CIS methods were used with the 6-31G(d,p) and/or 6-311++G(2d,2p) basis sets. [b] For atom numbering, see Figure 2.

The NH_3 internal rotation transition structure (denoted TS in Table 2) calculated at the SCF/6-31G(d,p) level is very slightly nonplanar. The motion from the minimum-energy structure toward the TS is mainly a rotation of the NH_3 molecule by 60° around the H-bond, combined with an in-plane wagging motion of 1.2°; that is, the H_O-O-N_2 angle changes from 3.9° to 5.1°. The calculated energy difference between the TS and the minimum-energy structure is 25.8 cm^{-1}. This purely electronic barrier height for internal rotation does not take into account the changes of vibrational zero-point energy along the internal rotation path. A one-dimensional (1D) quantum-mechanical calculation of the torsional level structure is presented in Section 2.6.

The CIS calculation predicts that $S_1 \leftarrow S_0$ electronic excitation leads to considerable changes of intra- and intermolecular bond lengths, analogous to those calculated for *cis*-7-HQ·$(H_2O)_2$.[39] The R(O···N) distance decreases by 0.053 Å. However, many

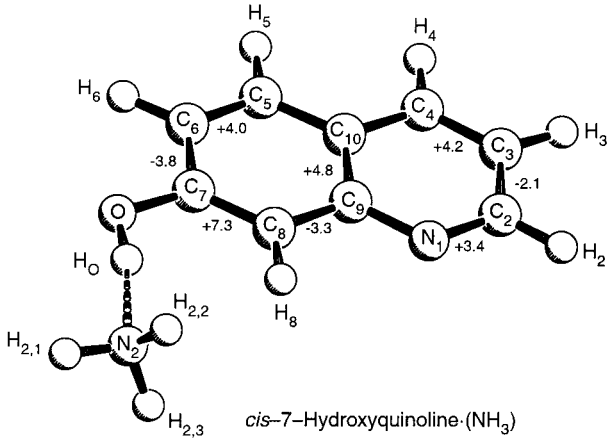

Figure 2. The calculated B3LYP/6-311++G(2d,2p) structure of *cis*-7-hydroxyquinoline·NH_3. The atom labels are employed for defining the structural parameters in Table 2 and in the text. The calculated bond length changes (in pm) occurring upon electronic $S_1 \leftarrow S_0$ excitation are given next to the bonds.

intramolecular C−C and C−N bonds are predicted to expand/contract by similar or even larger values, for example, the C_7-C_8 bond by +0.073 Å. Thus, although the O−H···N coordinate changes, major geometrical changes are *not* along the proton-transfer coordinate. Also, the O−H and the C═O bond lengths, which one expects to be directly involved in the proton-transfer coordinate, are predicted to change very little, by +0.003 and −0.019 Å, respectively. A detailed list of calculated S_1-state geometry parameters and bond length changes is given in Table 2. The calculated bond length changes are also shown in Figure 2 next to the bonds.

2.4. Dipole Moments and Charge Distribution. It is interesting to examine the calculated charge distributions of the *cis*-7-HQ·NH_3 complex in the S_0 and S_1 states. The calculated dipole moment of the complex increases from 1.88 D in the S_0 state [SCF/6-31G(d,p)] to 3.32 D in the S_1 state [CIS/6-31G-(d,p)]. This increase is in qualitative agreement with the observed increases in H-bond well depth, intermolecular vibrational frequencies, force constants, and torsional barriers which are observed experimentally (see below). To obtain a more detailed view of the charge flows upon $S_1 \leftarrow S_0$ excitation, we calculated the *differences* of the Mulliken charges, Δq_i, between the S_0 state (SCF) and the S_1 state (CIS) at each atom. The largest change, by −0.151 *e*, occurs at atom C_4 (see Figure 2), which is *far removed* from the H-bonding site. The next largest changes are, in order of decreasing magnitude, at C_3 (+0.064 *e*), C_{10} (−0.058 *e*), C_2 (−0.055 *e*), and C_7 (+0.035 *e*). The H-bonded O and H_O atoms show smaller changes of +0.042 and +0.009 *e*, respectively. Thus, the increase in H-bond well depth and curvature is not reflected in a charge flow directly to the hydrogen-bonded −O−H group, that is, a localized electrostatic interaction. It seems to be due to a more favorable medium-range interaction with the increased molecular dipole moment of the quinoline frame, driven by the $\pi-\pi^*$ transition.

2.5. Harmonic Intermolecular Vibrations. Six low-frequency intermolecular modes occur in the *cis*-7-HQ·NH_3 complex; the rocking mode ρ_1, the wagging mode β_1, and the intermolecular stretch σ originate from the translational degrees of freedom of the ammonia molecule (see Figure 3), and the β_2 wag, the ρ_2 rock, and the low-frequency torsion mode τ around the H-bond axis correlate with the three rotations of the free NH_3 molecule (see Figure 4). The wagging modes β_1 and β_2 and the σ stretch are in-plane symmetric (a′) vibrations, whereas ρ_1, ρ_2, and τ are a″ out-of-plane modes. The intermolecular

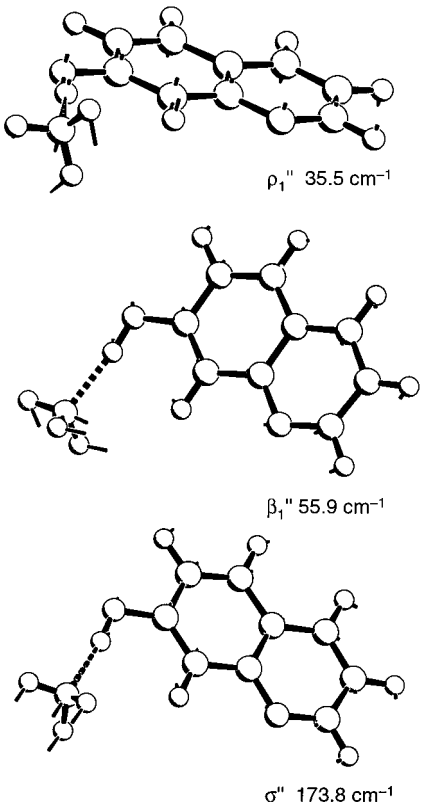

Figure 3. Perspective plots of the H-bond normal-mode eigenvectors of translational parentage of *cis*-7-HQ·NH_3, with the corresponding B3LYP/6-311++G(2d,2p) harmonic frequencies.

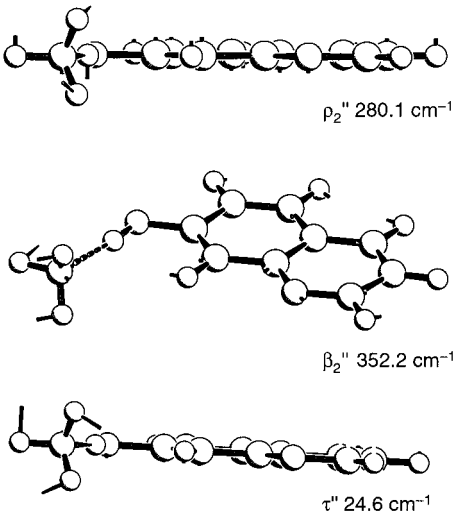

Figure 4. Perspective representations of the hydrogen-bond normal-mode eigenvectors of rotational parentage of *cis*-7-HQ·NH_3, with the B3LYP/6-311++G(2d,2p) harmonic frequencies.

vibrational eigenvectors of *cis*-7-HQ·NH_3 are shown in perspective views in Figures 3 and 4, together with the corresponding harmonic frequencies calculated at the B3LYP/6-311++G(2d,-2p) level of theory. The low-frequency intermolecular modes are fairly well decoupled from the 7-HQ frame; for the low-frequency β_1 and ρ_1 modes, the motions of the 7-HQ frame correspond to rigid-frame translation and/or rotation. However, the ρ_2 rocking mode involves an intramolecular O−H torsional contribution on 7-HQ, and the β_2 wag mode involves an O−H in-plane bend motion relative to the 7-HQ frame.

The calculated harmonic frequencies of the intermolecular modes calculated at the three levels of theory mentioned above

TABLE 3: Ab Initio Calculated Harmonic Frequencies of the *cis*-7-HQ·NH_3 Complex Using the SCF and B3LYP Methods for the S_0 State and the CIS Method for the S_1 State, with Either the 6-31G(d,p) and/or the 6-311++G(2d,2p) Basis Sets

		S_0 state			S_1 state
label	irreducible representation	SCF[b] 6-31G(d,p)	SCF[b] 6-311++G(2d,2p)	B3LYP 6-311++G(2d,2p)	CIS 6-31G(d,p)
τ	a″	30.8	30.9	24.6	46.1
ρ_1	a″	41.4	37.5	35.5	33.8
β_1	a′	54.8	49.6	55.9	62.2
ν_1	a″	122.9[b]	120.6[b]	122.3	118.1
σ	a′	165.4	142.4	173.8	177.5
ν_2	a″	186.1[b]	183.2[b]	185.0	170.3
ν_3/ρ_2[a]	a″	270.3	255.6	280.1	260.1
ν_4/β_2[a]	a′	300.7	279.5	289.9	218.4
ρ_2/ν_3[a]	a″	327.9	320.6	296.0	304.1
β_2/ν_4[a]	a′	364.3	354.4	352.2	376.0
ν_6	a″	411.4[b]	409.6[b]	415.4	365.1
ν_7/β_2[a]	a′	473.6	469.1	446.4	444.3
ν_8	a″	474.4[b]	472.5[b]	478.2	452.5
ν_9/β_2[a]	a′	531.2	526.1	495.9	507.7
ν_{10}	a′	526.7[b]	525.2	547.7	514.3
ν_{11}	a″	546.4[b]	537.9[b]	550.1	573.8
ν_{12}	a′	607.6[b]	606.6[b]	632.6	648.7
ν_{13}	a″	665.4[b]	655.4[b]	661.2	684.1
ν_{14}	a′	713.8[b]	710.4[b]	741.4	755.3
ν_{15}	a″	757.4[b]	721.7[b]	770.9	758.6
ν_{16}	a′	758.9[b]	754.4[b]	782.1	795.2
ν_{17}	a″	776.7[b]	761.9[b]	784.6	804.4
ν_{18}	a″	793.8[b]	780.9[b]	842.0	832.7
ν_{19}	a″	844.8[b]	836.7[b]	857.0	892.3

[a] Mixed inter/intramolecular vibrations; the preponderant vibrational motions are indicated. Note that the labeling follows the S_0-state sequence. [b] Intramolecular frequencies scaled with 0.9028, intermolecular frequencies unscaled.

are gathered in Table 3 and are compared with the experimental values (see below). With the exception of the τ and ρ_1 modes, the SCF/6-311++G(2d,2p) harmonic frequencies are consistently lower than those predicted by the other two calculations. This is in line with the lower interaction energy noted above.

As in 2-naphthol·H_2O[49] and 6-hydroxyquinoline·H_2O,[50] two intramolecular out-of-plane a″ modes ν_1 and ν_2 at 122.3 and 185.0 cm^{-1} [B3LYP/6-311++G(2d,2p)] fall within the intermolecular frequency range. These two low-frequency modes are observed as combination bands (see below) and can couple with the low-frequency out-of-plane a″ ρ_1 and ρ_2 modes of *cis*-7-HQ·NH_3. The ρ_2 and β_2 modes cannot be unequivocally separated from the intramolecular modes ν_3 (a″) and ν_4 (a′), respectively. These mixed intra/intermolecular vibrations are labeled in Table 3 with the predominant motion first; that is, ν_3/ρ_2 is predominantly ν_3 with a noticeable ρ_2 component.

2.6. The τ Internal Rotation Potential and Torsional States. The torsional mode τ (see Figure 4) has a low reduced mass, because of the light H atoms, and a large associated rms vibrational amplitude. Combined with the low barrier for the internal rotation of NH_3 relative to the 7-HQ frame calculated above, the harmonic approximation is inappropriate. To calculate the torsional (internal rotation) level structure, we applied a one-dimensional (1D) anharmonic approach, assuming approximate separability of the vibrational Hamiltonian in normal coordinates. We assume that the torsional coordinate τ ($0-2\pi$) is a rigid-body rotation of NH_3 around its figure axis in the calculated minimum-energy structure of the complex, neglecting precessional or nutational motions of the NH_3 figure axis around the O···N direction. More elaborate treatments of this problem have been recently developed.[51,52] The assumption of separability of the torsional mode is also implicit in the torsion−rotation analysis of the spectra of *trans*- and *cis*-2-naphthol·NH_3 and *trans*-1-naphthol·NH_3.[40,41] For the phenol·NH_3 complex, Schiefke et al.[53] calculated the 1D internal rotation levels, using a barrier calculated at the SCF 6-31G(d,p) level, but did not compare the results to their vibronic spectra. Separability was also assumed in the treatment of the internal rotation of the H_2O moiety in the complexes phenol·H_2O[42,54−57] and 2-naphthol·H_2O.[49]

TABLE 4: Calculated NH_3 Internal Rotation (Torsional) Levels in the S_0 and S_1 States of *cis*-7-Hydroxyquinoline·NH_3, Using the 1D Potential and Parameters Given in the Text

no./irreducible representation	S_0 state	S_1 state	no./irreducible representation	S_0 state	S_1 state
zero-point energy	18.7	20.8	$3A_2$	36.0	39.4
$0A_1$	0.00	0.00	$3A_1$	53.3	62.4
1E	0.18	0.10	4E	62.9	70.1
2E	32.7	37.3	5E	84.2	91.4

For the 1D potential energy function along τ, the Fourier expansion[58]

$$V_\tau = V_3(1 - \cos 3\tau)/2 + V_6(1 - \cos 6\tau)/2 + V_9(1 - \cos 9\tau)/2 + ...$$

is employed, where the V_n terms denote the n-fold barrier contributions. Usually, one finds that $|V_3| \gg |V_6| \gg |V_9|$, and we truncate the expansion after the first term. The reduced internal rotational constant F of *cis*-7-HQ·NH_3 was calculated assuming rigid-body internal rotation of NH_3 around its C_3 axis, in the calculated geometry of the complex, giving $F = 6.637$ cm^{-1}. The analogous values determined by Pratt and co-workers were $F = 6.62 \pm 0.05$ cm^{-1} for *trans*-1-naphthol·NH_3, $F = 6.59 \pm 0.05$ cm^{-1} for *cis*-2-naphthol·NH_3, and $F = 6.58 \pm 0.05$ cm^{-1} for *trans*-2-naphthol·NH_3.[40,41]

The 1D internal rotation Schrödinger equation[58] was solved numerically, resulting in the eigenvalues given in Table 4. The torsional levels are labeled by the angular momentum quantum number l (appropriate for the low-barrier limit) and the irreducible representation in C_{3v}. The ′ and ″ labels used later

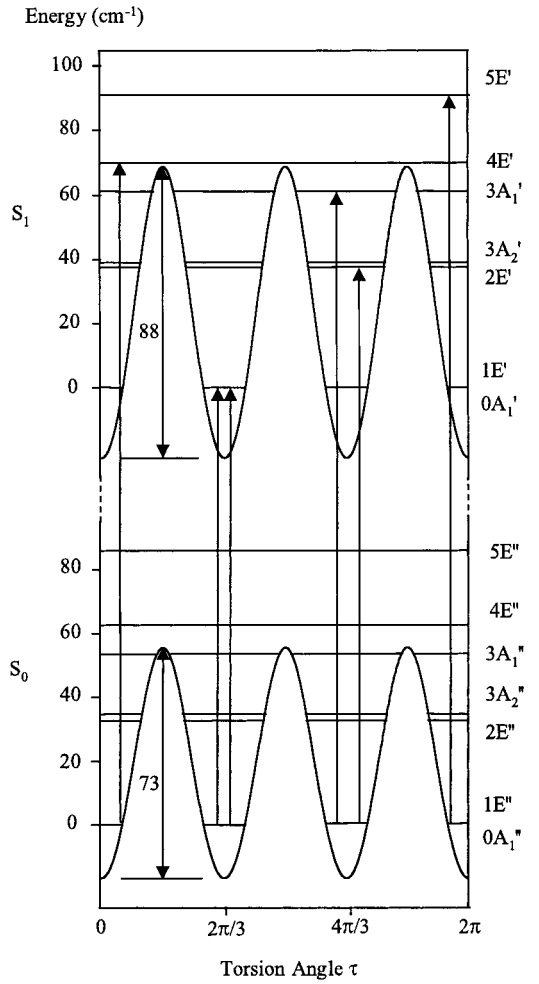

Figure 5. S_0 and S_1 excited-state effective one-dimensional torsional potentials as a function of torsion angle τ with barrier heights $V_3(S_0)$ and $V_3(S_1)$. The calculated S_0 and S_1 torsional levels are indicated, using the reduced rotation constant $F = 6.637$ cm^{-1}. Optically allowed transitions from the 0A″ and 1E″ levels are indicated by arrows. Note that the E levels are degenerate and that the $0A_1/1E$ splitting of ~0.1 cm^{-1} is not visible on this scale.

in the text refer to the S_1 and S_0 states, respectively. The *effective* 1D barrier heights in the ground state and electronically excited state, $V_\tau(S_0)$ and $V_\tau(S_1)$, were fitted to experimental torsional transition frequencies (see the analysis below), assuming that F is identical in both states. This yielded $V_\tau(S_1) = 88 \pm 1$ cm^{-1} and a ground-state barrier height $V_\tau(S_0) = 73 \pm 1$ cm^{-1}. These two torsional potentials and their calculated torsional levels up to $l = 5$ are shown in Figure 5.

The calculated SCF/6-31G(d,p) torsional barrier of 25.8 cm^{-1} is substantially lower than the effective 1D S_0-state barrier derived from the spectroscopic analysis. There are several reasons for this: (1) The SCF 6-31G(d,p) method yields an R(O··N) which is too long by nearly 0.1 Å, judging from the B3LYP/6-311++G(2d,2p) calculation. (2) The ab initio saddle-point optimization yields a stationary point of the full $3N - 6$ dimensional space. In contrast, the model employed above refers to a 1D rigid internal rotation, which constrains the torsional path and increases the effective barrier. (3) The geometrically calculated F is only an approximation to the F that would result from integrating the full mass-weighted torsional path in $3N - 6$ dimensions.[51,52]

3. Experimental Results

3.1. Experimental Setup. 7-HQ·NH_3 complexes were synthesized and cooled in a 20 Hz pulsed supersonic expansion of NH_3/neon (0.5%/99.5%) at 1.0−1.4 bar backing pressure; typical pulse widths were 200 μs fwhm. 7-HQ (Kodak) was placed in a magnetically actuated pulsed nozzle (0.4 mm diameter) heated to 193 °C. Two-color resonant two-photon ionization (2C-R2PI) spectra were recorded by crossing the skimmed supersonic jet at ~90° with unfocused (~3 mm diameter) UV excitation and ionization laser beams. $S_1 \leftarrow S_0$ excitation was performed with a frequency-doubled DCM dye laser (50−900 μJ/pulse), pumped by the second harmonic of a Nd:YAG laser. For the ionization step, a second pulsed UV dye laser was used (Rhodamine 6G/MeOH mixture) with an intensity of ~1.8 mJ/pulse, pumped by a second Nd:YAG laser. Ionization was performed closely above the ionization potential (IP) at 285 nm (see below). Other experimental details were described previously.[39,50,59]

The photoionization yield curve of *cis*-7-HQ·NH_3 was measured by fixing the excitation laser at the electronic origin of the cis rotamer at 29 925 cm^{-1} and scanning the ionization laser frequency across the steplike onset of ion signal. This onset yields an approximate adiabatic IP of 64 485 cm^{-1}. For all 2C-R2PI experiments, the ionization laser frequency was tuned just above the IP of the cis isomer, at 36 364 cm^{-1}. Dissociation of the 7-HQ·NH_3 to 7-HQ was found to be negligible (<1%). Because the ion signal of the *trans*-7-HQ·NH_3 was weak even at the electronic origin, no IP was determined for this rotamer.

For the dispersed fluorescence experiments, an excitation laser energy of 250 μJ/pulse was used. The laser beam crossed the jet beam about 4 mm downstream from the nozzle. The emitted fluorescence radiation was collected using quartz optics, dispersed with a SPEX 1704 1.0 m monochromator, and detected using a cooled Hamamatsu R928 side-on photomultiplier.

3.2. Intermolecular Vibrations. An overview of the 2C-R2PI spectrum of 7-HQ·NH_3 is presented in Figure 6. The first intense band observed in the spectrum at 29 925 cm^{-1} is assigned as the electronic origin of *cis*-7-HQ·NH_3. A weak band observed at 29 790 cm^{-1}, 135 cm^{-1} to the red, with only 2.5% of the intensity of the cis rotamer, is tentatively assigned to the electronic origin of the *trans*-7-HQ·NH_3 rotamer. This is based on analogous assignments for *trans*- and *cis*-2-naphthol·H_2O[60] and for *trans*- and *cis*-2-naphthol·NH_3.[40] Similar assignments have been given for the closely related complexes *trans*- and *cis*-6-hydroxyquinoline·H_2O[50] and *trans*- and *cis*-7-hydroxyquinoline·H_2O.[35,39]

This assignment is also supported by the SCF/6-31G(d,p) calculated energy differences which predict that the trans rotamer lies at higher energy than the cis, with ΔE_{rel}(trans − cis) = 1.88 kcal/mol. At the source temperature of 466 K, this translates into a trans/cis Boltzmann ratio of ~1:8. This is higher than the observed ratio of 1:40 but is of the right order of magnitude. We note that this ratio is lower for the bare 7-HQ molecule, for which, based on the calculated E_{rel}(trans − cis), the trans/cis rotamer ratio is 1:4 at $T = 470$ K.[61] If the weak band at 29 790 cm^{-1} is the trans electronic origin, one may safely assume that the associated vibronic band structure is even weaker and that all intense bands observed above 29 925 cm^{-1} are due to the *cis*-7-HQ·NH_3 rotamer.

With these assignments, the spectral red shifts of the electronic origins of 7-HQ upon complexation with NH_3 amount to $\Delta\nu = -754.3$ cm^{-1} (2.16 kcal/mol) for the trans rotamer and $\Delta\nu = -917.6$ cm^{-1} (2.62 kcal/mol) for the cis rotamer. These values represent the increases of the H-bond dissociation energy upon electronic excitation, $\Delta\nu = D_0(S_0) - D_0(S_1)$. Both

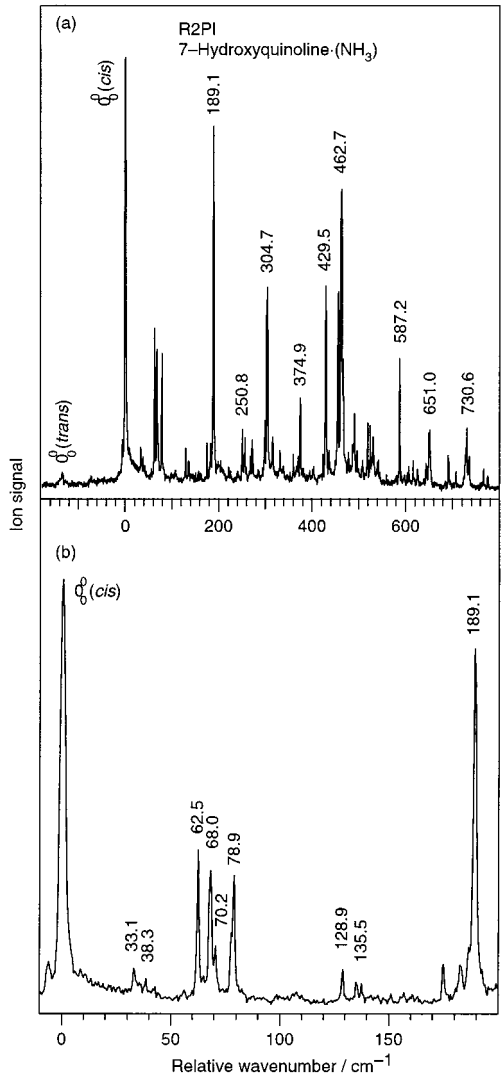

Figure 6. (a) Two-color resonant two-photon ionization spectrum of 7-hydroxyquinoline·NH_3. The wavenumber scale is relative to the cis-rotamer electronic origin at 29 925 cm^{-1}. (b) The expanded spectrum up to 0_0^0 +200 cm^{-1}, showing the low-frequency bending, rocking, and torsional transitions (see text).

TABLE 5: Properties of the Hydrogen-Bonded Complexes of NH_3 with *trans*-1-Naphthol, *cis*-2-Naphthol, *trans*-2-Naphthol, and the *cis*-7-HQ·NH_3 Complex in the S_0 and S_1 States

		V_3 (cm^{-1})		R(O···N) (Å)	
labels	$\Delta\nu$ (cm^{-1})	S_0	S_1	S_0	S_1
trans-1-naphthol·NH_3[a]	−236.4	39.9	46.5	2.86	2.72
cis-2-naphthol·NH_3[a]	−586.3	41.1	53.8	2.87	2.71
trans-2-naphthol·NH_3[a]	−626.3	34.2	58.2	2.88	2.68
cis-7-hydroxyquinoline·NH_3	−917.5	73.0	88.0	2.835[b]	2.782[c]

[a] Data from refs 40 and 41. [b] B3LYP/6-311++G(2d,2p) R_e value. [c] ΔR_e[CIS/6-31G(d,p) − SCF/6-31G(d,p)] + R_e(B3LYP/6-311++G-(2d,2p)).

spectral shifts are larger than those of *cis*-2-naphthol·NH_3 (−586.3 cm^{-1}) and *trans*-2-naphthol·NH_3 (−626.3 cm^{-1}) and much larger than that of *trans*-1-naphthol·NH_3 (−236.4 cm^{-1}); see also Table 5.[1,2,5,40,41]

In the $S_1 \leftarrow S_0$ 2C-R2PI spectra, low-frequency excitations of *cis*-7-HQ·NH_3 appear at 0_0^0 +63, +68, +79, and +189 cm^{-1}, as indicated in Figure 6. They are assigned to intermolecular excitations, because the lowest intramolecular excitations

TABLE 6: Experimental Vibrational Frequencies (in cm^{-1}) and Assignments for *cis*-7-Hydroxyquinoline·NH_3 in the S_0 and S_1 States, from Fluorescence and Two-Color R2PI Spectra

S_0 state			S_1 state	
assignment	freq	intensity[a]	assignment	freq
			ρ_1'	33.1
τ_{2E}^{1E}	31.2	0.7	τ_{1E}^{2E}	38.3
			τ_{0A}^{3A}	62.5
τ_{3A}^{0A}	54.2	5.7	β_1'	68.0
β_1''	59.6	5.4	τ_{1E}^{4E}	70.2
$2\rho_1''$	71.4	1.4	$2\rho_1'$	78.9
			$\tau_{0A}^{3A} + \beta_1'$	128.9
			$2\beta_1'$	135.5
				174.9
			$3\beta_1'$	182.8
σ''	172.1	16.4	σ'	189.1
$\nu_1'' + \nu_2''$	275.4	1.9	$\sigma' + \tau_{0A}^{3A}$	250.8
ν_4''	281.7	2.9	ν'_4	303.1/304.7
$\sigma'' + 2\beta_1''$	294.9	1.4	$\sigma' + \tau_{0A}^{3A} + \beta_1'$	315.8
$2\sigma''$	334.3	0.9		
β_2''	347.1	3.4	$2\sigma'$ or β_2'	374.9
ν_7''	442.0	8.3	ν_7'	429.5
			$2\sigma' + 2\rho_1'$	455.9
ν_9''	491.2	14.4	ν_9'	462.7
$\sigma'' + \beta_2''$	516.2	2.0	$\sigma' + \nu'_4$	490.7
ν_{10}''	546.2	5.9	ν'_{10}	519.0
$\nu_7'' + \sigma''$	614.2	0.7	$\nu_9' + \tau_{0A}^{3A}$	524.4
ν_{12}''	628.0	4.8	ν'_{12}	587.2
			$\nu_7' + \sigma'$	616.5
	649.3	1.4	$\nu_9' + \sigma'$	651.0
$2\beta_1''$	706.7	0.9		691.6
ν_{16}''	783.0	16.4	ν'_{14}	730.6
	826.0	0.9	$\nu'_4 + \nu_9'$	765.9

[a] Intensity of electronic origin = 100.

in the $S_1 \leftarrow S_0$ spectra of bare 7-HQ lie >280 cm^{-1} above the origin. A number of intramolecular excitations are also apparent and are assigned by comparison to the *cis*-7-HQ R2PI spectrum. The band frequencies relative to 0_0^0 are given in Table 6; the assignments are discussed below.

The dispersed fluorescence emission spectrum obtained following excitation at the electronic origin of *cis*-7-HQ·NH_3 is shown in Figure 7. In the low-frequency region of 0−300 cm^{-1}, bands at 0_0^0 +54, +60, +71, +172, and +282 cm^{-1} are attributed to intermolecular vibrations. A number of intramolecular vibrations are observed at higher frequencies (e.g., 282, 347, 442, 491, 546, 628, and 783 cm^{-1}). Frequencies relative to the 0_0^0 band together with the calculation results are given in Table 6. The S_1 fluorescence lifetime at the electronic origin was measured to be 6.3 ± 1 ns. Using the integrated absorption band strength in solution, we estimate the quantum yield of this complex to be quite low, $\Phi_{fl} = 0.10 \pm 0.03$.

3.2.1. Stretching Vibrations. In both the $S_1 \leftarrow S_0$ 2C-R2PI and $S_1 \rightarrow S_0$ fluorescence spectra, we find that the electronic/vibrational selection rules for C_s symmetry are followed; that is, transitions occur only to a′ fundamentals, overtones, or combination levels. This is in agreement with the ab initio calculated C_s symmetric structures for both the S_0 and S_1 states. In analogy to *cis*- and *trans*-2-naphthol·NH_3,[5] *cis*- and *trans*-2-naphthol·H_2O,[49] and 6-HQ·H_2O,[50] we assign the most intense intermolecular band at +189.1 cm^{-1} in the R2PI spectrum to the S_1 intermolecular stretching fundamental σ'. The harmonic frequency from the CIS calculation is $\sigma' = 177.5$ cm^{-1}. The $2\sigma'$ overtone is tentatively identified at 374.9 cm^{-1}.

In the fluorescence spectrum, the intense band at 172.1 cm^{-1} is assigned as the intermolecular stretching fundamental σ''; this

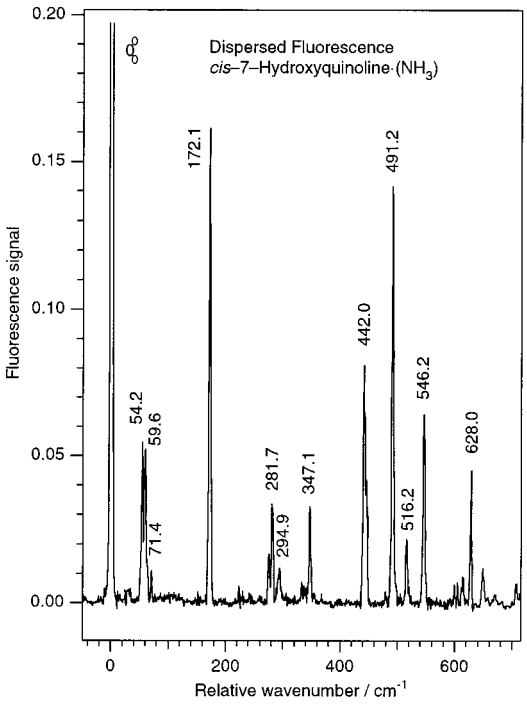

Figure 7. Dispersed fluorescence spectrum of *cis*-7-hydroxyquinoline·NH_3, excited at the electronic origin at 29 925 cm^{-1}, with a monochromator band-pass of 3.6 cm^{-1}. The wavenumber scale is relative to the 0_0^0 band. The electronic origin is off the scale at 1.0 relative units.

is the most intense transition up to 900 cm^{-1}. The harmonic σ'' frequency was calculated as 173.8 cm^{-1} with the B3LYP/6-311++G(2d,2p) method and as 165.8 cm^{-1} at the SCF/6-31G-(d,p) level (see Table 3). The former frequency especially is in excellent agreement, considering that anharmonicity should lower the harmonic frequency. The calculated intermolecular stretching frequency is substantially higher than that for the *cis*-7-HQ·H_2O complex. Thus, the higher binding and dissociation energies are paralleled by a higher stretching force constant.

3.2.2. Wagging, Rocking, and Torsional Vibrations. The β_1 (a′) wagging mode is allowed as a fundamental in the $S_1 \leftrightarrow S_0$ electronic transitions. In both the R2PI and fluorescence spectra, a group of bands is observed in the 50−80 cm^{-1} region. In the dispersed fluorescence spectrum, there are two equally intense bands at +54.2 and +59.6 cm^{-1}, followed by a weaker band at +71.4 cm^{-1} (see Figure 7). The B3LYP/6-311++G(2d,2p) harmonic β_1'' frequency is 55.6 cm^{-1}. We assign the *second* band, at +59.6 cm^{-1}, to the β_1'' fundamental, for reasons given below.

In the R2PI spectrum, there is a group of bands at +62.5, +68.0, +70.2, and +78.9 cm^{-1} (see Figure 6b). Again, we assign the second band of the group at 68.0 cm^{-1} as β_1'. The CIS harmonic frequency is $\beta_1' = 62.2$ cm^{-1}. The overtone $2\beta_1'$ is weakly observed at 135.5 cm^{-1}. A weak band at 182.8 cm^{-1} is tentatively assigned to the second harmonic $3\beta_1'$, enhanced by Fermi resonance with the intermolecular stretch. The alternative assignment of β_1' to the band at 62.5 cm^{-1} is possible; however, we would then expect an overtone at or slightly lower than 125 cm^{-1}, which is not observed.

The *first* band in each group is attributed to a torsional (internal rotation) transition; in absorption, this is $\tau(3A_1' \leftarrow 0A_1'')$, calculated at 61.6 cm^{-1} and observed at 62.5 cm^{-1}. Note that experimentally there is no overtone at twice the 62.5 cm^{-1} excitation, as would be expected for the torsional vibration. In fluorescence, the analogous $\tau(0A_1' \rightarrow 3A_1'')$ is calculated at 53.2 cm^{-1} and observed at 54.2 cm^{-1}. In both absorption and emission, the band intensities are enhanced by Fermi resonance of the torsional levels with the close-lying β_1' and β_1'' states, respectively.

On the basis of the torsional barriers derived from the two assignments above (see also Table 4), other torsional transitions can be predicted and compared to experiment. Thus, the 1E″ state is predicted to lie only 0.18 cm^{-1} above the 0A″ ground state; hence, it is thermally populated even at the low vibrational/rotational temperature of the supersonic jet. E′ ← E″ torsional transitions can arise in absorption, as indicated in Figure 5. The splitting of the electronic origin due to the two torsional subbands $0A_1' \leftarrow 0A_1''$ and 1E′ ← 1E″ is calculated to be only 0.08 cm^{-1}, which is below our laser resolution of ∼0.3 cm^{-1}. The 2E′ ← 1E″ transition is predicted at 37.1 cm^{-1}; indeed, a weak band is observed at 38.3 cm^{-1} in the R2PI spectrum. The 4E″ ← 1E″ transition is predicted to lie at 69.1 cm^{-1}; we assign the shoulder on the high-frequency side of the 68 cm^{-1} R2PI band at 70.2 cm^{-1} to this transition. The $\tau(3A_1' \leftarrow 0A_1'')$ torsional transition also appears in combination with β_1' at 128.9 cm^{-1} (see Table 6).

When exciting at the electronic origin with our laser bandwidth of 0.3 cm^{-1}, both the $0A_1' \leftarrow 0A_1''$ and 1E′ ← 1E″ torsional subbands are simultaneously excited. Hence, fluorescence from the 1E′ level should give rise to weak torsional transitions in emission; the 1E′ → 2E″ fluorescence transition calculated at 32.8 cm^{-1} (see Table 4) is assigned to a weak band observed at ∼31 cm^{-1}.

For β_2'', the B3LYP/6-311++G(2d,2p) harmonic frequency of 352.2 cm^{-1} is in good agreement with a fluorescence band observed at 347.1 cm^{-1}. The bare *cis*-7-HQ molecule does not exhibit any fluorescence bands in this region, which favors assigning this transition to an intermolecular mode. An alternative would be the $2\sigma''$ overtone. In the R2PI spectrum, we assign an intense band at +374.9 cm^{-1} (see Figure 6) as the β_2' vibration; again, assignment as the $2\sigma'$ overtone is possible.

Both the intermolecular rocking modes ρ_1 and ρ_2 are a″ in C_s. They are symmetry-forbidden as fundamentals in the $S_1 \leftrightarrow S_0$ transitions but may occur as sequence or overtone bands. The *third* strong band in each group, at 78.9 cm^{-1} (R2PI) and +71.4 cm^{-1} (fluorescence), is assigned to the $2\rho_1'$ or $2\rho_1''$ overtone, respectively. These overtones are enhanced by Fermi resonance with the β_1' and β_1'' states, respectively. Analogous $\beta_1 \leftrightarrow 2\rho_1'$ Fermi resonances also occur in the spectra of *cis*- and *trans*-6-HQ·H_2O.[50] The large-amplitude motions associated with these a″ rocking vibrations give rise to a dipole moment modulation, rendering them weakly allowed, with selection rules similar to Herzberg−Teller bands. Hence, weak a″ fundamentals may be observed in the spectra. The calculated S_0- and S_1-state ρ_1 frequencies are 35.5 and 33.8 cm^{-1}, respectively. A weak R2PI band at 33.1 cm^{-1} may be assigned as the ρ_1^0 transition.

3.3. Discussion. The σ stretching and the low-frequency β_1 wag frequencies of *cis*-7-HQ·NH_3 can be compared with those of *cis*-2-naphthol·NH_3 in both the S_0 and S_1 states[5] (see Table 7). In both electronic states, the frequencies of *cis*-7-HQ·NH_3 are 7−8% higher, implying stronger curvature of the O−H··· N hydrogen-bond stretching and wagging potentials.

More information on the stretching potentials can be derived within a pseudodiatomic model.[62−64] The intermolecular stretching coordinate is assumed to be a 1D motion, and the 7-HQ and NH_3 subunits are taken as pseudoatoms of mass 17.03 and 145.19 amu, giving a reduced mass $\mu = 15.242$ amu. We assumed Morse potential functions for both electronic states. For S_0, we employ the B3LYP well depth $D_e(S_0) = 2990.6$ cm^{-1}

TABLE 7: Comparison of Selected Intermolecular Vibrational Frequencies (cm^{-1}) for the Hydrogen-Bonded Complexes of NH_3 with *trans*-1-Naphthol, *cis*-2-Naphthol, *trans*-2-Naphthol, and the *cis*-7-HQ·NH_3 Complex in the S_0 and S_1 States

labels	β_1	σ	k_σ	ω_e	$\omega_e x_e$
cis-2-naphthol·NH_3,[a] S_0	53.2	160.9	23.2		
cis-2-naphthol·NH_3,[a] S_1	56.9	175.6	27.6		
cis-7-hydroxyquinoline·NH_3, S_0	59.6	172.1	28.25	177.37	2.630
cis-7-hydroxyquinoline·NH_3, S_1	68.0	189.1	33.77	193.91	2.400

[a] Data from ref 5.

(8.550 kcal/mol) (see Table 1). For a Morse function, the fundamental frequency is given by $\omega_e - 2\omega_e x_e$. Combining this with $\sigma'' = 172.1\ cm^{-1}$ and the relation $\omega_e x_e = \omega_e^2/4D_e$ yields the harmonic frequency $\omega_e(S_0) = 177.4\ cm^{-1}$, the anharmonicity constant $\omega_e x_e(S_0) = 2.630\ cm^{-1}$, the Morse potential stiffness parameter $a(S_0) = 1.5419\ Å^{-1}$, and the 1D dissociation energy $D_0(S_0) = 2902.6\ cm^{-1}$. The S_1-state Morse potential was obtained using the experimental spectral red shift $\Delta\nu = D_0(S_0) - D_0(S_1) = -917.5\ cm^{-1}$, giving $D_0(S_1) = 3820.1\ cm^{-1}$. Using the experimental anharmonic fundamental stretching frequency $\sigma' = 189.1\ cm^{-1}$, the well depth is determined as $D_e(S_0) = 3916.4\ cm^{-1}$, giving $\omega_e(S_1) = 193.9\ cm^{-1}$, $\omega_e x_e(S_1) = 2.400\ cm^{-1}$, and $a(S_1) = 1.4732\ Å^{-1}$. These Morse potential parameters are gathered in Table 7.

From the ω_e values, the harmonic S_0- and S_1-state stretching force constants are calculated to be $k_\sigma'' = 28.25$ and $k_\sigma' = 33.77$ N/m, respectively. These force constants are 22% larger than the $k_\sigma'' = 23.2$ and $k_\sigma' = 27.6$ N/m of the *cis*-2-naphthol·NH_3 complex (see Table 7). For most H-bonded gas-phase dimers, the pseudodiatomic stretching force constants are considerably smaller, in the range between 10 and 20 N/m.[62−64] Using the same pseudodiatomic approximation, the H-bond stretching force constant for pyrimidine···H−OH was recently determined to be 13.8 N/m.[65]

The relative displacement of the S_0- and S_1-state Morse potentials along the intermolecular stretching coordinate was calculated, using the observed ratio of Franck−Condon factors for the σ_1^0 and origin bands in fluorescence, $I(\sigma_1^0)/I(0_0^0) = 0.164$ (see Table 6). (The σ_0^1 transition in the 2C-R2PI spectrum is saturated and cannot be employed.) The anharmonic stretching wave functions were calculated by numerical solution of the 1D vibrational Schrödinger equation with the Morse potentials and reduced mass determined above, followed by numerical quadrature to give the Franck−Condon factors for the 0_0^0 and σ_1^0 transitions. This yielded a displacement of the potential minima along the stretching coordinate of ±0.063 Å. Structure determinations on the 1- and 2-naphthol·NH_3 complexes indicated *contractions* of the H-bond upon electronic excitation by 0.16−0.2 Å[40,41] (see also Table 5). The CIS calculation of *cis*-7-HQ·NH_3 also indicates a bond contraction, albeit by only −0.053 Å (see Table 2). Hence, we assume contraction of the H-bond upon electronic excitation (i.e., −0.063 Å). This experimental value obtained within the pseudodiatomic model using Morse potentials is very close to the ab initio calculated value.

Pratt and co-workers determined the V_3 barriers of the analogous *trans*-1-naphthol·NH_3, *cis*-2-naphthol·NH_3, and *trans*-2-naphthol·NH_3 complexes from a detailed rotational analysis of the 0A′ ← 0A″ and 1E′ ← 1E″ subbands of the $S_1 \leftarrow S_0$ electronic origin, using an effective torsional−rotation Hamiltonian.[40,41] The V_3 values they derived were in the range of 34−41 cm^{-1} for the S_0 state and 46−58 cm^{-1} for the S_1 state; see Table 5 and refs 40 and 41. The torsional barriers of *cis*-7-HQ·NH_3 determined here, $V_3(S_0) = 73$ and $V_3(S_1) = 88\ cm^{-1}$, are up to twice as high. They were determined directly from the torsional transition frequencies in the vibronic spectra (four torsional transitions in absorption and two frequencies in emission). The higher barriers in *both* electronic states of 7-HQ·NH_3 imply stronger intermolecular interactions, presumably due to repulsive interactions of the atoms $H_{2,2}$ and $H_{2,3}$ of NH_3 with the H_8 atom of 7-hydroxyquinoline. This is in line with the higher β_1 wag and σ stretching frequencies and the larger spectral red shift of 7-HQ·NH_3, compared to the naphthol complexes. The *increase* in the effective 1D torsional barrier by 15 cm^{-1} upon excitation to the S_1 state can be understood in terms of the decrease of R(O···N) by −0.06 Å (see above), which brings these two ammonia H atoms into closer contact with the H_8 atom.

One might argue that the effective V_3 barriers determined for the 1- and 2-naphthol·NH_3 complexes in refs 40 and 41 differ from those determined for 7-HQ·NH_3 because of the different type of data and different analysis (torsion−rotation vs torsion). However, for all three complexes, the analysis is based on a model 1D hindered internal rotation *ansatz*, neglecting couplings to the other inter- and intramolecular modes (stretching, wag, rocking, and N−H symmetric stretch). Our F constant for internal rotation was based on the ab initio geometry for the S_0 state and was retained for the S_1 state, and it is very close to the F values of *trans*-1-naphthol·NH_3, *cis*-2-naphthol·NH_3, and *trans*-2-naphthol·NH_3. Also, any alternative band assignments to torsional transitions of *cis*-7-HQ·NH_3 would *increase* the torsional barriers beyond the values derived above. Thus, we believe that the differences of torsional barriers between the 7-HQ·NH_3 and the 1- and 2-naphthol·NH_3 complexes are significant.

4. Conclusions

$S_1 \leftrightarrow S_0$ vibronic spectra of the 7-hydroxyquinoline·NH_3 complex were measured using 2C-R2PI and fluorescence emission spectroscopy. These allow the characterization of a number of H-bond stretching, wagging, and torsional vibrational excitations in the S_0 and S_1 states, which are relevant to the discussion of the (incipient) proton-transfer coordinate of this and the larger 7-hydroxyquinoline·$(NH_3)_n$ clusters.[36,37]

All bands of the R2PI and fluorescence spectra can be traced to the enol tautomer; there is no spectroscopic sign of the keto tautomer in the supersonic jet. Both trans and cis rotamers of the enol are observed. The trans/cis ratio in the supersonic jet is 1:40; that is, the trans rotamer is energetically disfavored relative to the cis rotamer, even more so than for bare 7-hydroxyquinoline, for which the trans/cis rotamer ratio is about 1:5.[35,61]

The H-bond topology corresponds to the O−H···NH_3 and not to the NH_3···N or NH_3···O H-bond configurations. Ab initio structure optimizations using SCF/6-31G(d,p), CIS/6-31G(d,p), and the B3LYP/6-311+1G(2d,2p) hybrid density functional methods all yielded C_s-symmetric S_0- and S_1-state minimum-energy structures, with a nearly linear H-bond for both the cis and the trans rotamers, similar to the 1- and 2-naphthol·NH_3[40,41] and the 6- and 7-hydroxyquinoline·H_2O complexes.[37,39] At the B3LYP level, the hydrogen bond length R(O···N) is predicted to be 2.835 Å, close to the ⟨R⟩(O···N) values of 2.86−2.88 Å determined for the 1- and 2-naphthol·NH_3 complexes by Pratt et al.[41]

Normal-mode analyses were carried out with a main focus on the six intermolecular modes, characterized as the a′ H-bond stretch σ, the a″ H-bond torsion τ, two a′ wags β_1 and β_2, and

two a″ rocks ρ_1 and ρ_2. The B3LYP harmonic frequencies are in very good agreement with experiment for both inter- and intramolecular vibrations. The scaled SCF frequencies are slightly inferior.

The S_0-state H-bond stretching frequency $\sigma'' = 172$ cm^{-1} is already relatively high and increases by about 10% to 189 cm^{-1} in the S_1 state. The harmonic stretching force constant, derived in the framework of a pseudodiatomic model, is $k''_\sigma = 28.3$ N/m, increasing to $k'_\sigma = 33.8$ N/m in the S_1 state. In parallel, the H-bond dissociation energy increases by 2.62 kcal/mol upon $S_1 \leftarrow S_0$ excitation, corresponding to ∼40% of the B3LYP calculated ground-state dissociation energy $D_0(S_0) = 6.78$ kcal/mol.

The H-bond stretching vibration Franck−Condon factors imply that the R(O···N) distance changes by ±0.063 Å during the $S_1 \leftrightarrow S_0$ transition. The CIS (S_1-state) calculation predicts a contraction of the R(O···N) distance by −0.053 Å relative to the SCF (S_0-state) calculation, in good agreement with the experiment. The picture that emerges is that $S_1 \leftrightarrow S_0$ excitation deepens the H-bond well substantially, thereby increasing its curvatures and force constants. The H-bond length shortens, but *not* by a large amount. The observed/calculated contractions of 0.06/0.05 Å are 3−4 times smaller than the 0.2 Å contractions proposed for the analogous 1- and 2-naphthol·NH_3 complexes.[40,41] In the latter studies, the observed differences between the S_0- and S_1-state rotational constants were modeled in a way that attributes the geometry changes mainly to the shortening of the H-bond length, a procedure that should be viewed with some caution. The present CIS and SCF calculations on 7-HQ·NH_3 indicate that upon electronic excitation substantial geometry changes occur throughout the hydroxyarene framework (see Figure 2) and are *not* predominantly along the intermolecular R(O···N) coordinate.

The torsional τ mode was treated using a 1D internal rotation $V_\tau = V_3(1 - \cos 3\tau)/2$ periodic potential. On the basis of several observed excitations in the 30−70 cm^{-1} range, effective V'_3 and V''_3 barrier heights were determined. These barriers are higher than those determined by rotationally resolved spectroscopy for the 1- and 2-naphthol·NH_3 complexes.[40,41] With respect to every property measured (stretching, wagging, torsional frequencies, torsional barrier, and spectral red shift (see Tables 5 and 7)), the *cis*-7-hydroxyquinoline O−H···NH_3 hydrogen bond is stronger than those for the analogous 1- and 2-naphthol·NH_3 complexes. However, it clearly does *not* exhibit a proton-transfer reaction in either the S_1 or S_0 state.

Acknowledgment. This work was supported by the Schweiz. Nationalfonds (Project No. 20-53932.98).

References and Notes

(1) Cheshnovsky, O.; Leutwyler, S. *Chem. Phys. Lett.* **1985**, *121*, 1.
(2) Cheshnovsky, O.; Leutwyler, S. *J. Chem. Phys.* **1988**, *88*, 4127.
(3) Cheshnovsky, O.; Knochenmuss, R.; Leutwyler, S. *Chem. Phys. Lett.* **1988**, *144*, 317.
(4) Solgadi, D.; Jouvet, C.; Tramer, A. *J. Phys. Chem.* **1988**, *92*, 3313.
(5) Droz, T.; Knochenmuss, R.; Leutwyler, S. *J. Chem. Phys.* **1990**, *93*, 4520.
(6) Jouvet, C.; Lardeux-Dedonder, C.; Richard-Viard, M.; Solgadi, D.; Tramer, A. *J. Phys. Chem.* **1990**, *94*, 5041.
(7) Breen, J. J.; Peng, L. W.; Willberg, D. M.; Heikal, A.; Cong, P.; Zewail, A. H. *J. Chem. Phys.* **1990**, *92*, 805.
(8) Steadman, J.; Syage, J. A. *J. Chem. Phys.* **1990**, *92*, 4630.
(9) Weller, A. *Ber. Bunsen-Ges. Phys. Chem.* **1952**, *56*, 662.
(10) Weller, A. *Ber. Bunsen-Ges. Phys. Chem.* **1956**, *66*, 1144.
(11) Ireland, J. F.; Wyatt, P. A. H. *Adv. Phys. Org. Chem.* **1976**, *12*, 131.
(12) Kim, S. K.; Li, S.; Bernstein, E. R. *J. Chem. Phys.* **1991**, *95*, 3119.
(13) Syage, J. A.; Steadman, J. *J. Chem. Phys.* **1991**, *95*, 2497.
(14) Steadman, J.; Syage, J. A. *J. Am. Chem. Soc.* **1991**, *113*, 6786.
(15) Syage, J. A. *J. Phys. Chem.* **1991**, *95*, 10326.
(16) Hineman, M. F.; Brucker, G. A.; Kelley, D. F.; Bernstein, E. R. *J. Chem. Phys.* **1992**, *97*, 3341.
(17) Syage, J. A.; Steadman, J. *J. Phys. Chem.* **1992**, *96*, 9606.
(18) Syage, J. A. *Chem. Phys. Lett.* **1993**, *202*, 227.
(19) Syage, J. A. *J. Phys. Chem.* **1993**, *97*, 12523.
(20) Hineman, M. F.; Kelley, D. F.; Bernstein, E. R. *J. Chem. Phys.* **1993**, *99*, 4533.
(21) Kim, S.; Breen, J. J.; Willberg, D. M.; Peng, L. W.; Heikal, A.; Syage, J. A.; Zewail, A. *J. Phys. Chem.* **1995**, *99*, 7421.
(22) Knochenmuss, R. *Chem. Phys. Lett.* **1998**, *293*, 191.
(23) Knochenmuss, R. *Chem. Phys. Lett.* **1999**, *305*, 233.
(24) Martrenchard-Barra, S.; Dedonder-Lardeux, C.; Jouvet, C.; Solgadi, D.; Vervloet, M.; Grégoire, G.; Dimicoli, I. *Chem. Phys. Lett.* **1999**, *310*, 173.
(25) Mason, S. F.; Philip, J.; Smith, B. E. *J. Chem. Soc. A* **1968**, 3051.
(26) Schulman, S.; Fernando, Q. *Tetrahedron* **1968**, *24*, 1777.
(27) Thistlethwaite, P.; Corkill, P. *Chem. Phys. Lett.* **1982**, *85*, 317.
(28) Thistlethwaite, P. *Chem. Phys. Lett.* **1983**, *96*, 509.
(29) Itoh, M.; Adachi, T.; Tokumura, K. *J. Am. Chem. Soc.* **1984**, *106*, 850.
(30) Tokumura, K.; Itoh, M. *J. Phys. Chem.* **1984**, *88*, 3921.
(31) Lavin, A.; Collins, S. *Chem. Phys. Lett.* **1993**, *204*, 96.
(32) Lavin, A.; Collins, S. *Chem. Phys. Lett.* **1993**, *207*, 513.
(33) Lavin, A.; Collins, S. *J. Phys. Chem.* **1993**, *97*, 13615.
(34) Bohra, A.; Lavin, A.; Collins, S. *J. Phys. Chem.* **1994**, *98*, 11424.
(35) Lahmani, F.; Douhal, A.; Breheret, E.; Zehnacker-Rentien, A. *Chem. Phys. Lett.* **1994**, *220*, 235.
(36) Bach, A.; Leutwyler, S. *J. Chem. Phys.* **2000**, *112*, 560.
(37) Bach, A.; Leutwyler, S. Unpublished work, 2000.
(38) Bach, A.; Coussan, S.; Müller, A.; Leutwyler, S. *J. Chem. Phys.* **2000**, *112*, 1192.
(39) Bach, A.; Leutwyler, S. *Chem. Phys. Lett.* **1999**, *299*, 381.
(40) Plusquellic, D. F.; Tan, X.-Q.; Pratt, D. *J. Chem. Phys.* **1992**, *96*, 8026.
(41) Humphrey, S. J.; Pratt, D. *J. Chem. Phys.* **1996**, *104*, 8332.
(42) Schütz, M.; Bürgi, T.; Leutwyler, S.; Fischer, T. *J. Chem. Phys.* **1993**, *98*, 3763.
(43) Inauen, A.; Hewel, J. W.; Leutwyler, S. *J. Chem. Phys.* **1999**, *110*, 1463.
(44) Müller, A.; Talbot, F.; Leutwyler, S. *J. Chem. Phys.* **2000**, *112*, 3717.
(45) Frisch, M. J.; et al. *Gaussian 94*, revision D.4; Gaussian, Inc.: Pittsburgh, PA, 1995.
(46) Valiron, P.; Mayer, I. *Chem. Phys. Lett.* **1997**, *275*, 46.
(47) Szalewicz, K.; Jeziorski, B. *J. Chem. Phys.* **1996**, *104*, 8821.
(48) Bürgi, T.; Droz, T.; Leutwyler, S. *Chem. Phys. Lett.* **1995**, *246*, 291.
(49) Schütz, M.; Bürgi, T.; Leutwyler, S.; Fischer, T. *J. Chem. Phys.* **1993**, *99*, 1469.
(50) Bach, A.; Hewel, J.; Leutwyler, S. *J. Phys. Chem. A* **1998**, *102*, 10476.
(51) Mohr, W. *Spektroskopische Effekte von Kernbewegungen grosser Amplitude in Molekülkomplexen*; Universität Bern: Bern, Switzerland, 1997.
(52) Mohr, W.; Leutwyler, S. *Mol. Phys.*, submitted for publication, 2000.
(53) Schiefke, A.; Deusen, C.; Jacoby, C.; Gerhards, M.; Schmitt, M.; Kleinermanns, K.; Hering, P. *J. Chem. Phys.* **1995**, *102*, 9197.
(54) Berden, G.; Meerts, W.; Schmitt, M.; Kleinermanns, K. *J. Chem. Phys.* **1996**, *104*, 972.
(55) Gerhards, M.; Schmitt, M.; Kleinermanns, K.; Stahl, W. *J. Chem. Phys.* **1996**, *104*, 967.
(56) Helm, R. M.; Vogel, H. P.; Neusser, H. J. *J. Chem. Phys.* **1998**, *108*, 4496.
(57) Schmitt, M.; Jacoby, C.; Kleinermanns, K. *J. Chem. Phys.* **1998**, *108*, 4486.
(58) Kroto, H. *Molecular Rotation Spectra*; Wiley: New York, 1972.
(59) Bürgi, T.; Droz, T.; Leutwyler, S. *J. Chem. Phys.* **1995**, *103*, 7228.
(60) Johnson, J.; Jordan, K.; Plusquellic, D.; Pratt, D. *J. Chem. Phys.* **1990**, *93*, 2258.
(61) Coussan, S.; Bach, A.; Leutwyler, S. *J. Phys. Chem. A*, submitted for publication, 2000.
(62) Legon, A. C.; Millen, D. J. *Faraday Discuss. Chem. Soc.* **1982**, *73*, 71.
(63) Legon, A. C.; Millen, D. J. *Chem. Rev.* **1986**, *86*, 635.
(64) Legon, A. C.; Millen, D. J. *Acc. Chem. Res.* **1987**, *20*, 39.
(65) Melandri, S.; Sanz, M. E.; Caminati, W.; Favero, P. G.; Kisiel, Z. *J. Am. Chem. Soc.* **1998**, *120*, 11504.